

ISSN Online: 2160-0422 ISSN Print: 2160-0414

CO₂ Back-Radiation Sensitivity Studies under Laboratory and Field Conditions

Ernst Hammel, Martin Steiner, Christoph Marvan, Matthias Marvan, Klaus Retzlaff, Werner Bergholz, Axel Jacquine

International Climate Research, A Citizen Research Group, Vienna, Austria Email: ernst@icr2025.org, steiner@icr2025.org

How to cite this paper: Hammel, E., Steiner, M., Marvan, C., Marvan, M., Retzlaff, K., Bergholz, W. and Jacquine, A. (2024) CO₂ Back-Radiation Sensitivity Studies under Laboratory and Field Conditions. *Atmospheric and Climate Sciences*, **14**, 407-428.

https://doi.org/10.4236/acs.2024.144025

Received: July 19, 2024 Accepted: October 6, 2024 Published: October 9, 2024

Copyright © 2024 by author(s) and Scientific Research Publishing Inc. This work is licensed under the Creative Commons Attribution International License (CC BY 4.0).

http://creativecommons.org/licenses/by/4.0/





Abstract

We measured the IR back radiation using a relatively low-cost experimental setup and a test chamber with increasing CO₂ concentrations starting with a pure N₂ atmosphere against a temperature-controlled black reference background. The results confirm estimations within this work and previous finding about CO2-induced infrared radiation saturation within realistic atmospheric conditions. We used this setup also to study thermal forcing effects with stronger and rare greenhouse gases against a clear night sky. Our results and their interpretation are another indication for having a more critical approach in climate modelling and against monocausal interpretation of climate indices only caused by anthropogenic greenhouse gas emissions. Basic physics combined with measurements and data taken from the literature allow us to conclude that CO₂ induced infrared back-radiation must follow an asymptotic logarithmic-like behavior, which is also widely accepted in the climate-change community. The important question of climate sensitivity by doubling current CO₂ concentrations is estimated to be below 1°C. This value is important when the United Nations consider climate change as an existential threat and many governments intend rigorously to reduce net greenhouse gas emissions, led by an ambitious European Union inspired by IPCC assessments is targeting for more than 55% in 2030 and up to 100% in 2050 [1]. But probably they should also listen to experts [2] [3] who found that all these predictions have considerable flaws in basic models, data and impact scenarios.

Keywords

Climate Change, Greenhouse Gases, CO₂ Backscatter, IR Radiation

1. Introduction

Our atmosphere mainly comprises radiative inactive diatomic molecules N2

78.08% and O_2 20.95% by volume. The remaining 0.97% consists primarily in Ar with 0.93%, CO_2 with 0.04% in volume, and traces of hydrogen, helium, and other noble gases, methane, nitrous oxide, and ozone. A variable but radiatively dominant part is water vapor, which is on average about 1% in volume at sea level. Greenhouse (GH) molecules absorb terrestrial IR radiation emitted by the surface as result of warming caused by the incoming solar radiation. Their absorption characteristics allow them to act in the retention of heat within the atmosphere and to ensure that the global mean temperature of the atmosphere supports biological life. This is commonly known as the greenhouse effect. Therefore, the IR active components are water vapor, carbon dioxide, methane, dinitrogen monoxide, and ozone, in decreasing order of effectiveness due to their concentrations.

The infrared IR transmission spectra of CO_2 over a path length of 100 meters is shown in **Figure 1** against the wavenumber, $1/\lambda = v/c$ (λ = wavelength, ν = frequency, c = velocity of light). The transmission T or transmittance is the extent by which the incident radiation at any wave number is transmitted by the sample. For opaque media T = 0 and complete transparent media T = 1.

In reflection-free media absorbance, A = 1 - T (transmittance) according to Kirchhoff's law, which also allows the propagation of the equality of long wave emissivity ε and absorptivity a_{lw} .

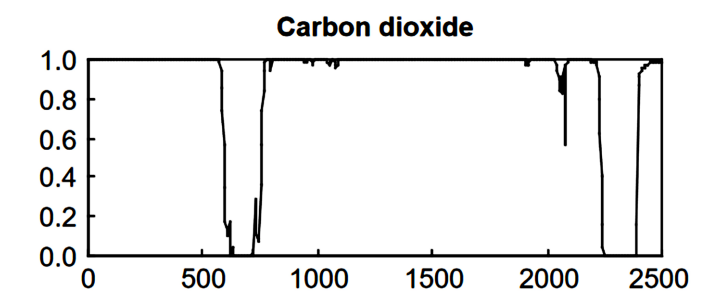


Figure 1. CO₂ IR Transmittance over 100 meters as a function of wavenumber from HITRAN [4].

The CO_2 spectrum is dominated by the bending vibration, centered at 667 cm⁻¹ equivalent to a wavelength of 14.992 μ m, and the asymmetrical stretching mode at 2349 cm⁻¹ equivalent to 4.257 μ m. The extra and very weak bands arise from further excitations and represent very small absorptions that are very often claimed to be significantly inaccurate calculations of the GH effect.

The surface has a mean global temperature of 288°K and its emission is approximated by a black body at this temperature, consisting of a continuous radiation spectrum unlike that of the GH gases which is specific for each molecule-species and made up of discrete rotation-vibrational bands. The continuous Planck or black body surface radiance is shown by the gray curve in **Figure 2** compared to the limits of the CO₂ absorption bands in orange and red of the main GH gas of CO₂.

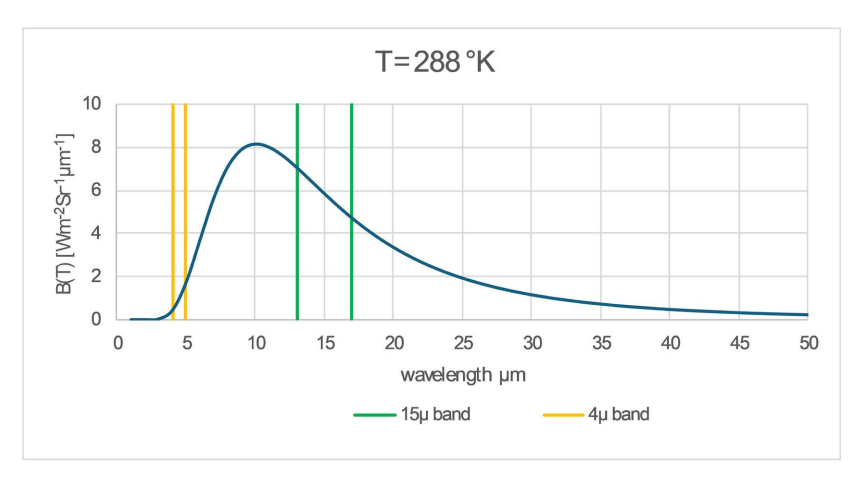


Figure 2. Black body radiator at T = 288°K and major CO₂ absorption bands.

The contribution of the 15 μ m and the 4 μ m CO₂ band to the total black body IR absorption can be estimated by integration of **Figure 1** with a rough maximum of 25%, where the major contribution comes from the 15 μ m band.

The solar irradiance intercepted by our atmosphere is $\pi a^2 S_0$, where α is the earth's radius. A fraction α , called the planetary albedo is reflected to space. The remaining portion is absorbed. Averaging over a long time over the total area of the globe, the absorbed solar radiation must be in balance with the radiation emitted by the atmosphere. In a very simplified 2D model we get according to Stefan-Boltzmann

$$\left(1 - \alpha\right) \frac{S_0}{4} = \sigma T_E^4 \tag{1}$$

where T_E is the theoretical emission temperature without any atmospheric greenhouse effect. Assuming on average $\alpha = 0.3$, we find $T_E = 255$ °K, a temperature much lower than the observed global average surface temperature of $T_S = 288$ °K. That means that the natural greenhouse effect results in additional $\Delta T_{GH} = 33$ °K, corresponding to

$$\sigma T_s^4 - \sigma T_F^4 = 150 \text{W/m}^2 \tag{2}$$

Detailed evaluation of the Planck function for T_s = 15°C or 288°K, results in the respective absorption bands.

13.26 - 17.07 μm (15 μ band), in energy densities of 9.22 \times 10⁻⁷ J/m³ or 17.6% of the total emission or 6.95 \times 10¹³ photons per m³.

4.19 - 4.38 μ m (4 μ band), in energy densities of 5.72 \times 10⁻⁹ J/m³, being 0.11% of the total emission or 1.22 \times 10¹¹ photons per m³.

From above considerations, we see that only the 15 μ band is significant with an IR absorption limited to $0.176 \times 391 \text{ W/m}^2 = 69 \text{ W/m}^2$ and back-radiation to $69/2 = 34.5 \text{ W/m}^2$. Simplified energy balance considerations in a single atmospheric layer are sketched in the following drawing. See **Figure 3**.

With $\varepsilon = 1$ we get

$$\sigma T_s^4 = U = 2\sigma T_A^4 = 2\sigma T_E^4 \tag{3}$$

and

$$T_{\rm S} = \sqrt[4]{2} \cdot T_{\rm F} \tag{4}$$

With $T_E = 255$ °K we therefore obtain $T_S = 303$ °K. This value is considerably higher than the observed 288°K. The discrepancy between theory and observation is explained by the fact that the atmosphere is not totally opaque to long-wave radiation. The presence of the atmosphere raises the temperature at the Earth's surface considerably. It is known that this effect is referred to as the greenhouse effect. We assume now that the atmosphere is semi-grey, *i.e.* it absorbs a constant fraction ε of the long-wave radiation, but is still transparent to solar radiation and emits upwards and downwards at a rate given by

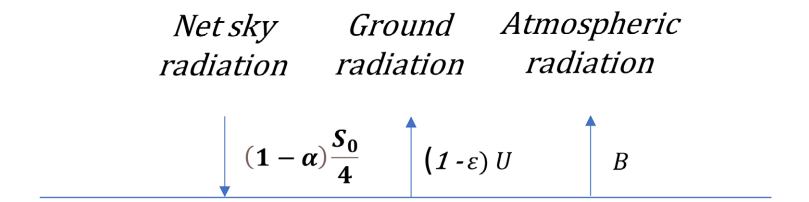
$$B = \varepsilon \sigma T_A^4 = \frac{\varepsilon}{2 - \epsilon} \sigma T_E^4 \tag{5}$$

where $\sigma T_{\scriptscriptstyle A}^{\scriptscriptstyle 4}$ is the radiation energy content of atmosphere. This leads to

$$T_S = \sqrt[4]{\frac{2}{2 - \epsilon}} \cdot T_E \tag{6}$$

With ε = 0.78, we then obtain T_S = 288°K. We can conclude that in this simplified model only 22% or 42.8 W/m² of the IR radiation gets directly to space and a net power balance of 152 W/m²—as expected from (2)—gets permanently recycled as part of the backscattered radiation.

For more appropriate multilayered atmospheres, we can take over the picture from the American Chemical Society (Figure 4).



Atmosphere, Temperature T_A

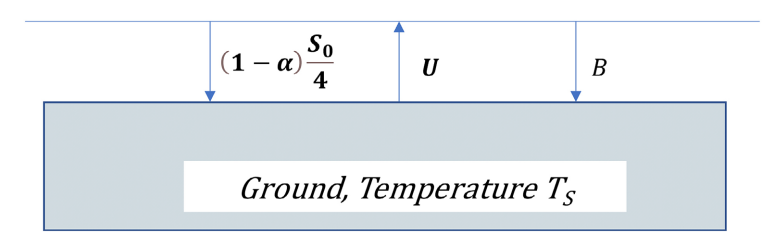


Figure 3. A single-layer model of the atmosphere, where S is the Solar irradiance, α is the cloud albedo and β the surface absorbance. U is the terrestrial radiation, of which a fraction $(1 - \varepsilon)$ penetrates directly through the atmosphere to space and B is the radiation emitted by the atmosphere [5].

Instead of using layered-atmosphere models, there exist excellent semi-

empirical formulas to be used. Night skies are shielded by clouds and humidity against radiation loss, while clear and dry conditions cannot compensate for strong radiation losses. This has been studied e.g. with the modified Swinbank model [7] [8].

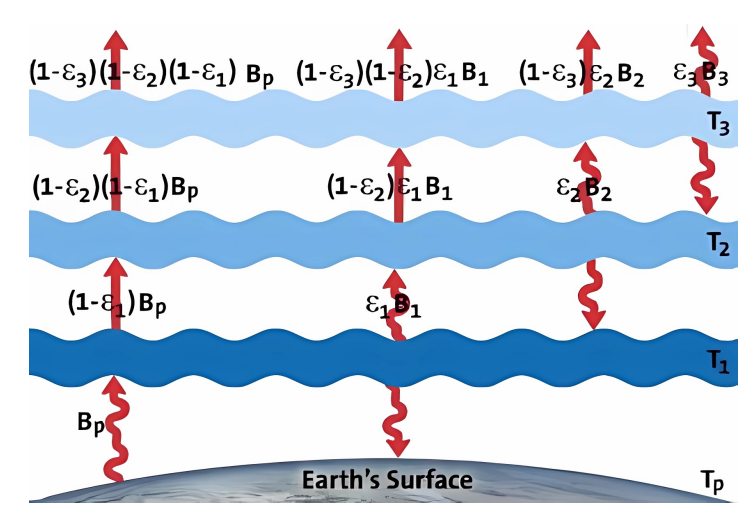


Figure 4. A multilayer atmosphere model illustrated here with three layers [6].

$$P_{SB} = (1 + KC^2) \cdot 8.78 \cdot 10^{-13} \cdot T_S^{5.852} \cdot RH^{0.07195}$$
 (7)

with

 P_{SB} upwards and downwards directed atmospheric radiation in W/m²

K $\,$ 0.34 clouds < 2 km, 0.18 for 2 km < altitude < 5 km, 0.06 for >5 km

C Cloud cover (0 clear skies, 1 covered skies)

T temperature in °K

RH relative humidity in %

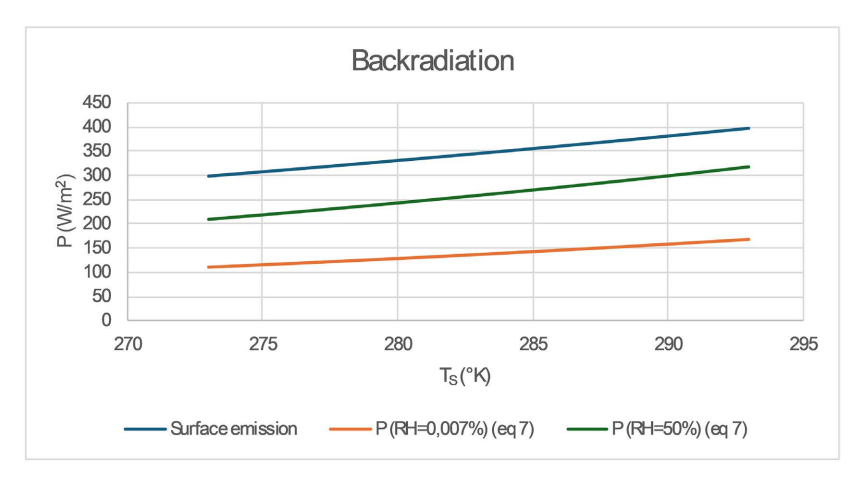
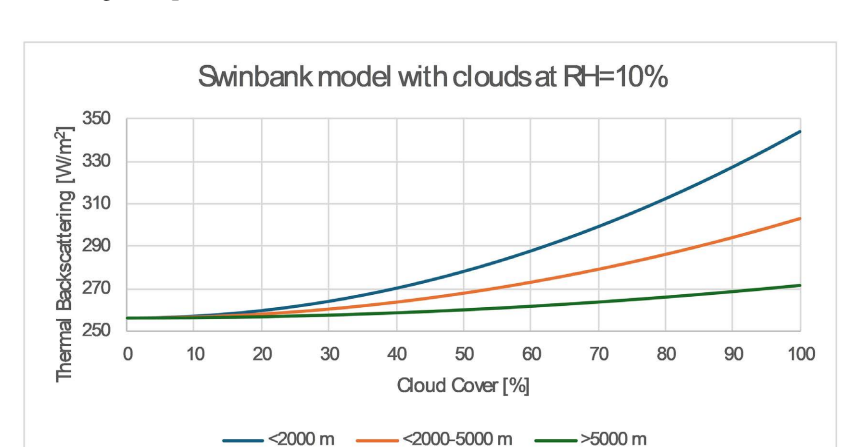


Figure 5. The effect of humidity on backward radiation compared between RH = 0.007% and RH = 50%. The blue line is the surface radiation at emissivity $\varepsilon_s \approx 0.95$ according to Stefan-Boltzmann.

As we can see in Figure 5, humidity has a strong impact and cloud coverage has



even stronger impact on the back-radiation.

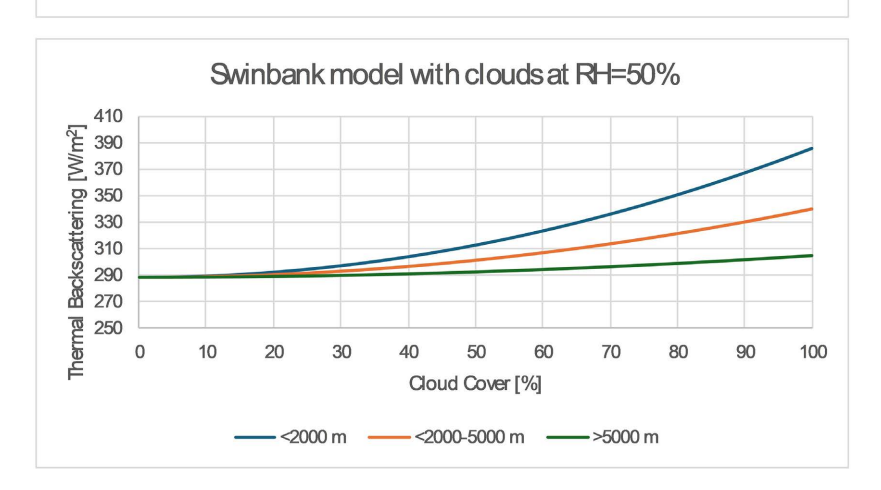


Figure 6. Thermal backward radiation characteristics of cloudy skies at RH = 10% and RH = 50%.

The last figures (**Figure 6**) suggest indeed that climate predictions depend critically on values like average relative humidity, cloud coverage, and albedo. These values vary considerably over the surface, depending on local temperature and geographic details. Gridded models can account for such values over years of observations to a certain extent only. Instabilities and risks due to erroneous positive feedback loop modeling and/or negligence of external geo-or astrophysical influences are obvious.

Data from ground measurements (**Figure 7**) indicate that the downward (backward) radiation of the atmosphere shows indeed full saturation of the IR CO₂ bands and does not support noticeable additional Thermal Forcing (TF) by increasing CO₂ in the lower atmosphere. It shows almost complete saturation of the 15 μ -central peak and close-to-saturation of the surrounding 15 μ band edges. Early studies [10] concluded as well that TF will not be significantly influenced by a further increase of atmospheric CO₂ (**Figure 8**). On the other hand, it is well known that concentrations below 50% of the current level would be detrimental to plant growth and climate.

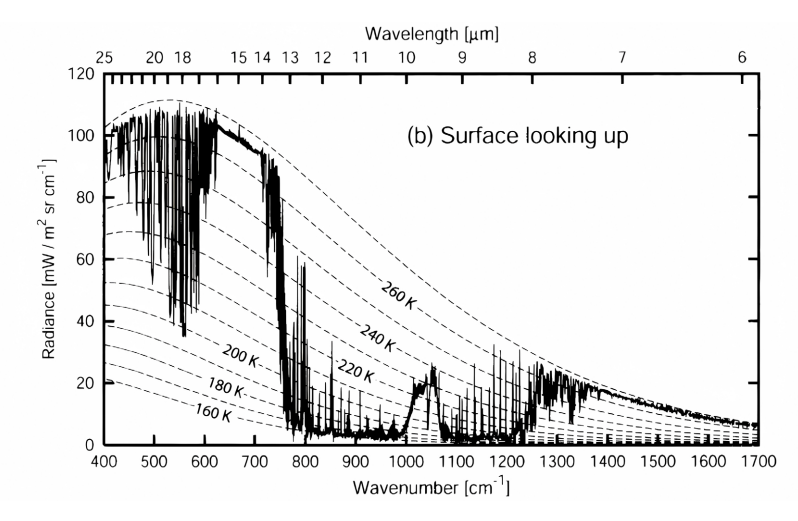


Figure 7. Measurements [9] of the infrared emission spectrum of the cloud-free atmosphere at the arctic surface looking upward.

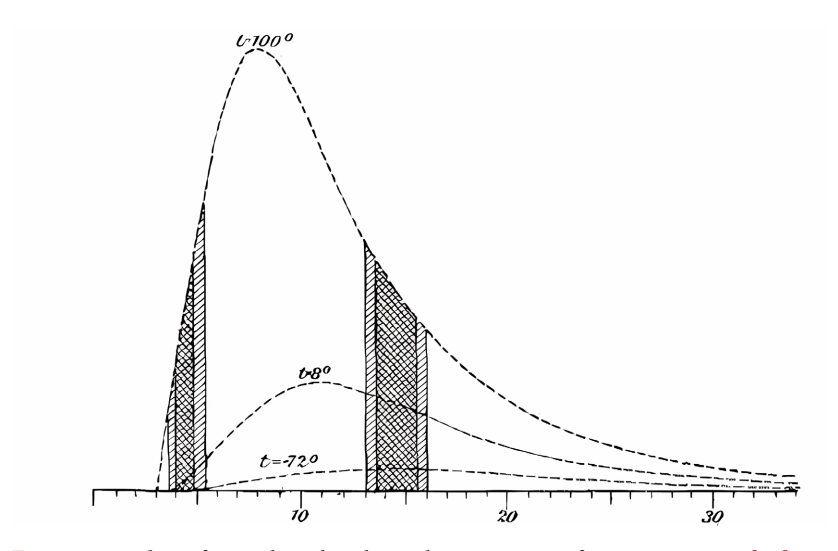


Figure 8. Studies of J. Koch at the Physical Department of Knut Angström [10].

The wavelength-dependent absorption $\ a_{\lambda}$ and re-emission is calculated from Beers Law, where transmission is exponentially reduced by increasing absorber thickness L

$$a_{\lambda}(L) = 1 - t_{\lambda}(L) = 1 - \frac{I_{\lambda}(L)}{I_{\lambda}(0)} = 1 - e^{-k(\lambda, L)}$$
(8)

Kirchhoff's law requires that absorbed radiation should get emitted again, or in other terms absorptivity should equal emissivity. For a limited wavelength window, $\Delta \lambda$ the specific emissivity $\varepsilon_{\Delta \lambda}$ (L) is therefore obtained by

$$\varepsilon_{\Delta\lambda}(L) = \frac{\int_{\lambda_{1}}^{\lambda_{2}} I_{\lambda}(0) \cdot a_{\lambda}(L) d\lambda}{\int_{0}^{\infty} I_{\lambda}(0) d\lambda}$$
(9)

where the spectral extinction coefficient a_{λ} is obtained from HITRAN or similar databases.

The significance of the unsaturated edges in 15 μ band is highly overestimated, as it can be easily shown that with an extinction < 3 they contribute only 0.17% to the full band when we consider their respective integrals (**Figure 9**). This has also been shown by Howard [11] used further in this study.

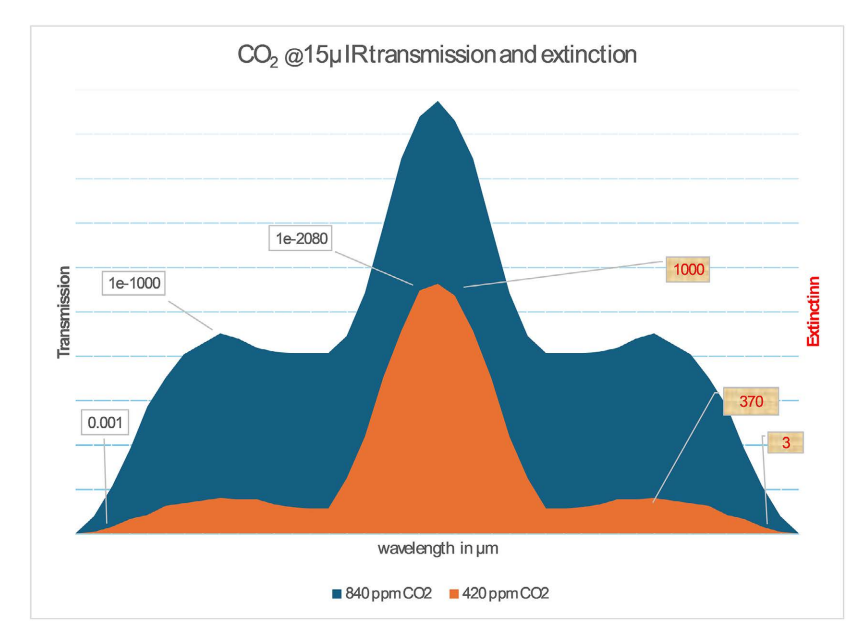


Figure 9. Transmission and Extinction Ratios in the 15 μ band.

The infrared (IR) spectra of the four main GH gases over a path length of 100 meters are presented in **Figure 10**, their concentrations being those that pertain to the atmosphere at sea level at 45% relative humidity.

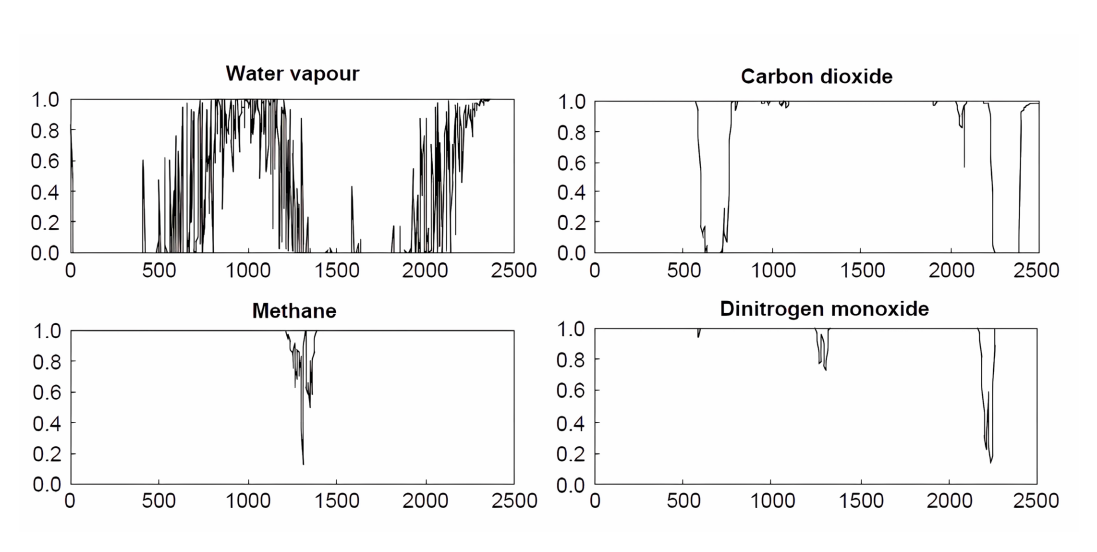


Figure 10. Infrared spectra of the main greenhouse gases as calculated using the HITRAN database; transmission is plotted against wavenumber (cm⁻¹) [4].

The 0 - 500 cm $^{-1}$ band of H₂O at 45% RH absorbs 66% of the surface IR radiation. The 1300 - 1800 cm $^{-1}$ band absorbs another 1%.

A 1 bar pressure atmosphere would have a theoretical thickness of 8.2 km. To visualize the effective column height of current CO₂ at different altitudes, we get the following Table 1.

Table 1. Equivalent of 400 ppm atmospheric CO₂ in meters at 1 bar atmospheric pressure.

H [m]	M(z)/M	1-M(z)/M	$\mathbf{L}_{\mathrm{CO}_2}^{\mathrm{up}}$ [cm]	L _{CO2} [cm]
0	0	1	344.83	0.00
500	0.06893722	0.93106278	321.06	23.77
1000	0.1331221	0.8668779	298.93	45.90
5000	0.51045834	0.48954166	168.81	176.02
10,000	0.76034896	0.23965104	82.64	262.19
20,000	0.94256738	0.05743262	19.80	325.03
30,000	0.98623621	0.01376379	4.75	340.08
40,000	0.99670149	0.00329851	1.14	343.69
¥	1	0	0.00	344.83

where we obtained the altitude-dependent mass M from the barometric formula

$$\frac{M[z]}{M} = 1 - e^{-\frac{z}{H}} \tag{10}$$

with H = 7 km. The total mass below the altitude z is calculated as

$$M(z) = \int_{0}^{z} \rho(z')dz' = \rho(0)H\left(1 - e^{-\frac{z}{H}}\right)$$
(11)

The thickness of the CO_2 -layer L_{CO_2} is a calculated value for a standard atmosphere at 1013.25 hPa and a total weight of 5.13×10^{15} tons of 8.21 km air at current 400 ppm. The table helps to understand the order of magnitudes when studying the atmospheric greenhouse effects of CO_2 . It also illustrates that 75% of the total CO_2 is contained within the troposphere below 10 km altitude and 95% is below 20 km. If we were to concentrate all the CO_2 (at 400 ppm) of an 8.2 km thick atmosphere with a pressure of 1 bar in a single column, the height of the column would be around 3.5 m. The optical path length of CO_2 IR radiation at these conditions is below 1 cm and therefore we can expect full saturation already at current concentrations.

From thermodynamics we get

$$\frac{dT}{dz} = \frac{\gamma - 1}{\gamma} mg / R \tag{12}$$

where $\gamma = \frac{c_P}{c_v}$ (e.g. 7/5 for dry air), m = 29 g/mol and *R* is the gas constant. For the International Standard Atmosphere with $\gamma = 1.26$ we obtain

 $\frac{dT}{dz}$ = -6.5 dK/km . Using this formula, we can estimate the LW back-radiation at

higher altitudes (**Figure 11**), when substituting the $T_s \to T_s - \frac{dT}{dz} \times \Delta z$.

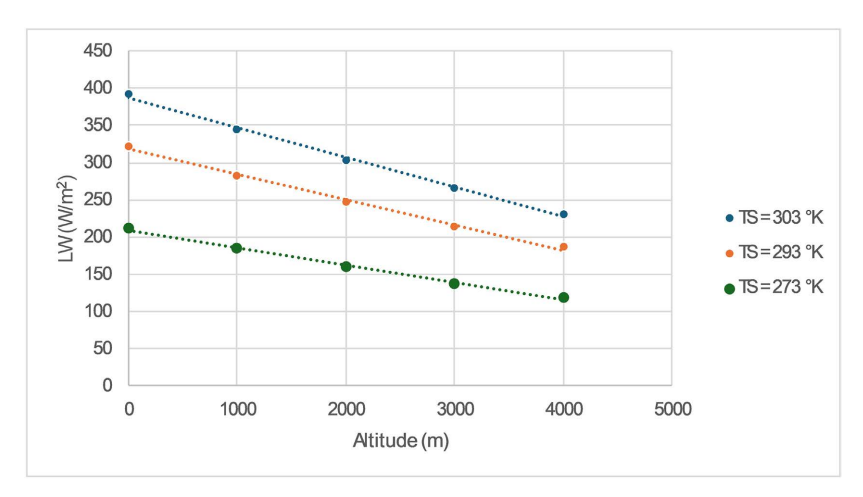


Figure 11. Estimated back-radiation in a standard atmosphere at three different surface temperatures.

This might be compared to measurements taken by a group from ETH Zurich in 1998 (Figure 12).

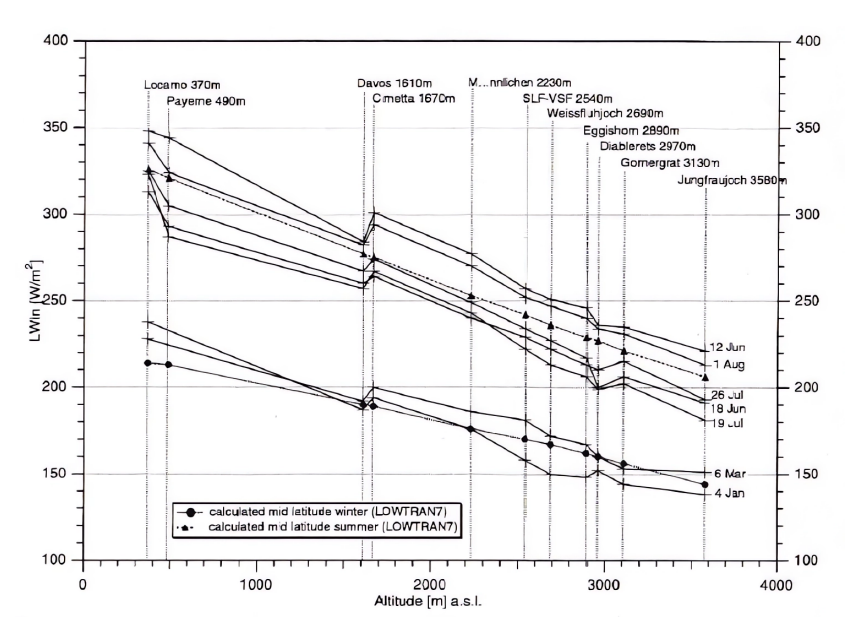


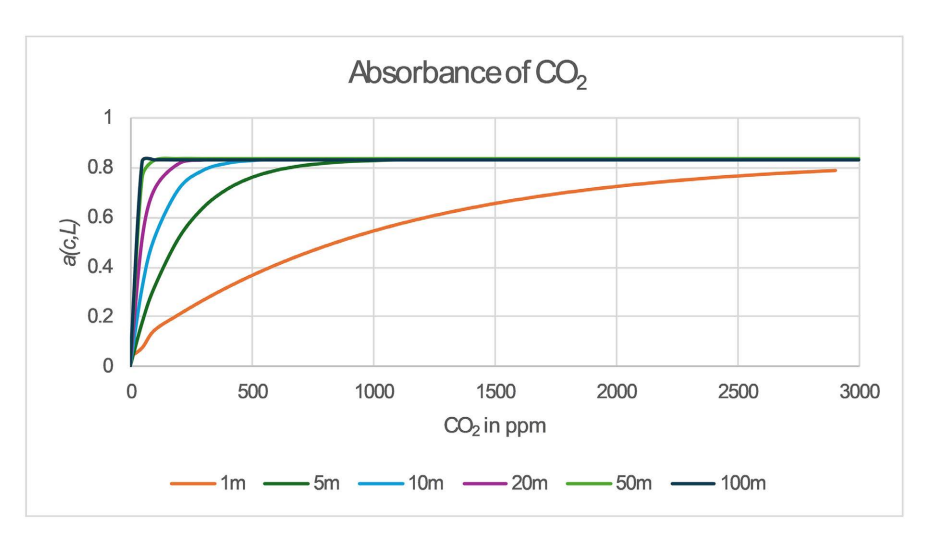
Figure 12. Altitude dependence of back-radiation with courtesy from C. Fröhlich [12].

The absorptivity a can be calculated using Beer's law for an infrared radiator from Equation (8) in a more generalized form.

$$a(c,L) = 1 - t(c,L) = 1 - \frac{I(c,L)}{I(c,0)} = 1 - e^{-k.c.L}$$
 (13)

From Akram [13] we can obtain $k = 1.82 \times 10^{-6} \text{ ppm}^{-1}\text{cm}^{-1}$ to calculate *a* as a function of *L*.

Figure 13 shows IR absorption saturation at current CO₂ levels already at air column length below 20 m. From this simple model, we must conclude that mechanisms other than CO₂ increases must explain significant atmospheric thermal



enhancement (ATE) in the total energy budget.

Figure 13. Absorbance of EMIRS200 IR light source in CO₂ from [13].

Howards [11] parameterizes the total absorption of strong lines at 15 μm and 4.3 μm according to

$$\int A_{\nu} d\nu = C + D \log w + K \log (p + P)$$
(14)

and

$$\overline{A} = \frac{\int A_{\nu} d\nu}{\nu_2 - \nu_1} \tag{15}$$

Substituting these values for $v_2 - v_1 = 250 \text{cm}^{-1}$ in the 15 µm band and $v_2 - v_1 = 340 \text{cm}^{-1}$ for the 4.3 µm band we obtain for a standard atmospheric layer of 1 km thickness (**Figure 14**) and for an 8.2 km thick atmosphere (**Figure 15**) as used for **Table 2**.

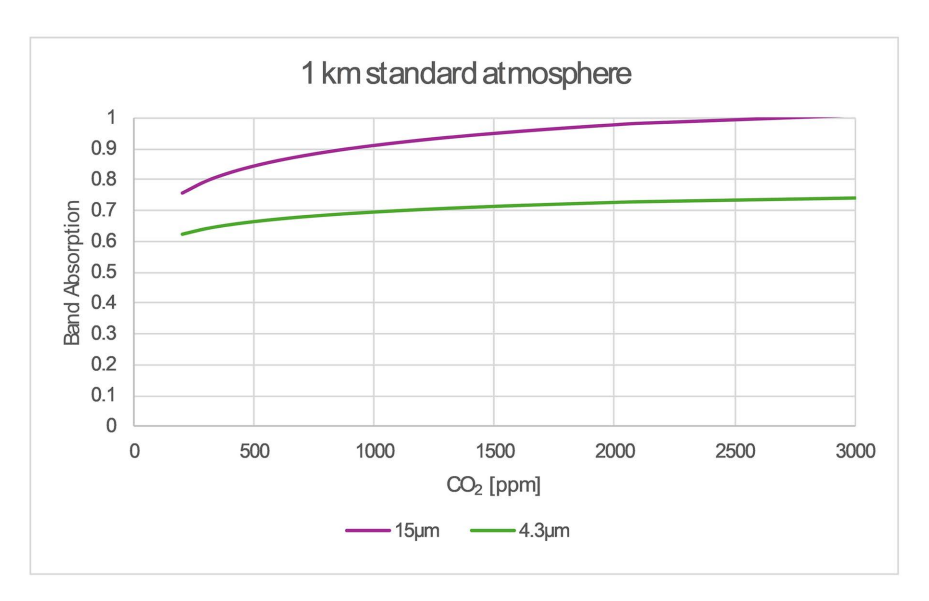


Figure 14. Band absorption within 1 km standard atmosphere [11].

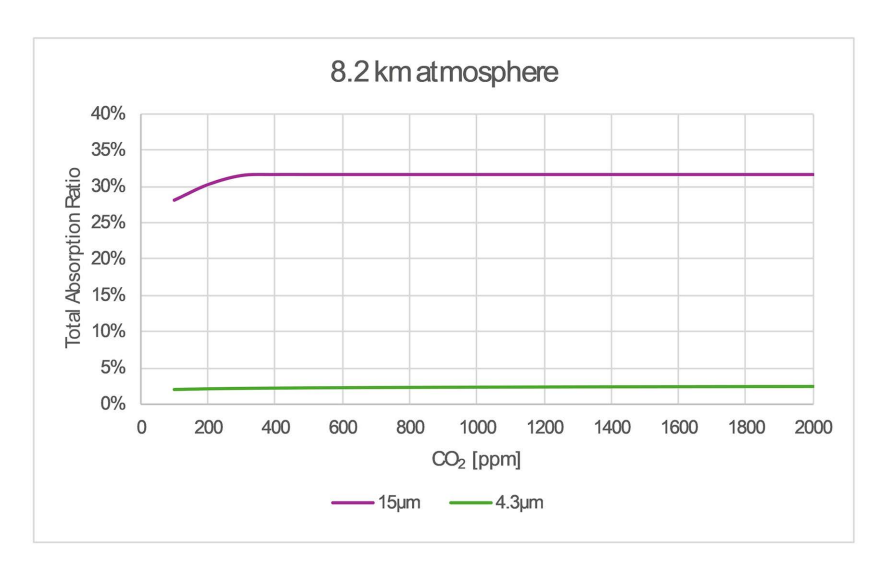


Figure 15. Absorption ratios for the two strong CO₂ absorption bands [11].

An increase from 400 to 800 ppm in CO_2 shows no measurable increase in IR absorption for the 15 μ and 4.3 μ bands and therefore total saturation. Other elaborate studies [14] estimate the total terrestrial long wavelength absorptivity a_{LW} .

$$a(L) = \frac{\int_0^\infty I_\lambda(0) \cdot a_\lambda(L) d\lambda}{\int_0^\infty I_\lambda(0) d\lambda} \times 100\%$$
 (16)

and obtain the following results for different latitudes.

Table 2. Calculated a_{LW} from Harde [14] for various CO₂ concentrations.

CO ₂ (ppm) –	absorptivities ε (%)						
	tropics	mid-latitudes	high-latitudes	average 3 zones	global mean		
0	81.90	69.44	58.98	74.68	77.02		
35	83.80	74.48	67.04	78.43	80.08		
70	84.18	75.35	68.32	79.10	80.62		
140	84.65	76.31	69.80	79.86	81.29		
210	84.99	77.00	70.77	80.40	81.76		
280	85.28	77. 51	71.52	80.83	82.14		
350	85.53	77.95	72.14	81.19	82.45		
380	85.65	78.12	72.38	81.34	82.58		
420	85.76	78.33	72.68	81.51	82.74		
490	85.91	78.67	73.16	81.80	83.00		
560	86.16	78.98	73.61	82.06	83.24		
630	86.35	79.29	74.02	82.32	83.46		
700	86.52	79.58	74.41	82.56	83.68		
770	86.69	79.85	74.78	82.79	83.88		

The next figure (**Figure 16**) shows the global mean values of the table above. While our previous model neglected the layered structure by assuming an isobar atmosphere, Harde [14] was taking the barometric effects into account.

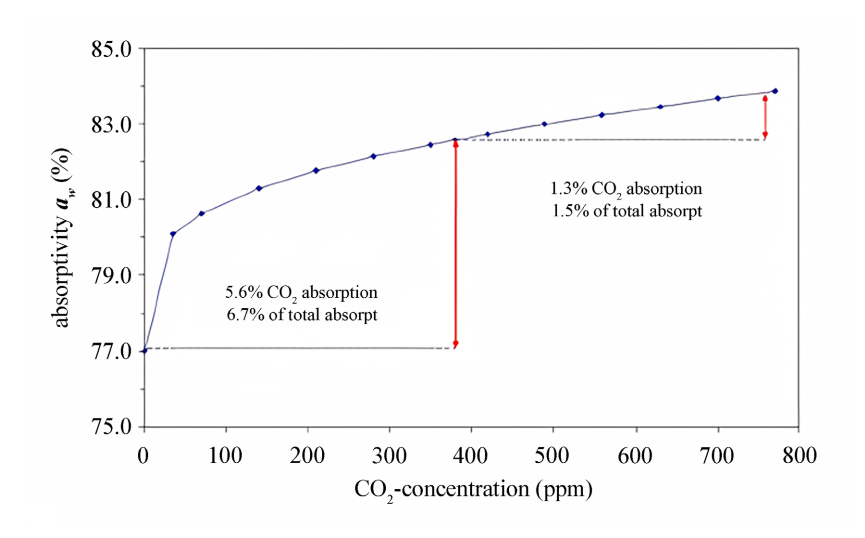


Figure 16. Influence of doubling CO₂ concentration on total absorptivity [14].

This study shows an upper limit of additional ATE by 1.5%. Average surface temperatures of T_s = 288°K correspond to 390 Wm⁻² black body radiation. From the foregoing considerations, we learned that doubling CO₂ atmospheric concentrations from 400 to 800 ppm amounts to a maximum 1.5% change of energy absorbed in the atmosphere, *i.e.* a maximal 3 Wm⁻² of back-radiation increase. Using the Stefan-Boltzmann formula we then obtain a first estimation of a corresponding temperature increase or GH contribution of 0.5°K by having 800 ppm atmospheric content compared to the current 400 ppm. This also corresponds very well with the results from Wijngaarden and Happer [2].

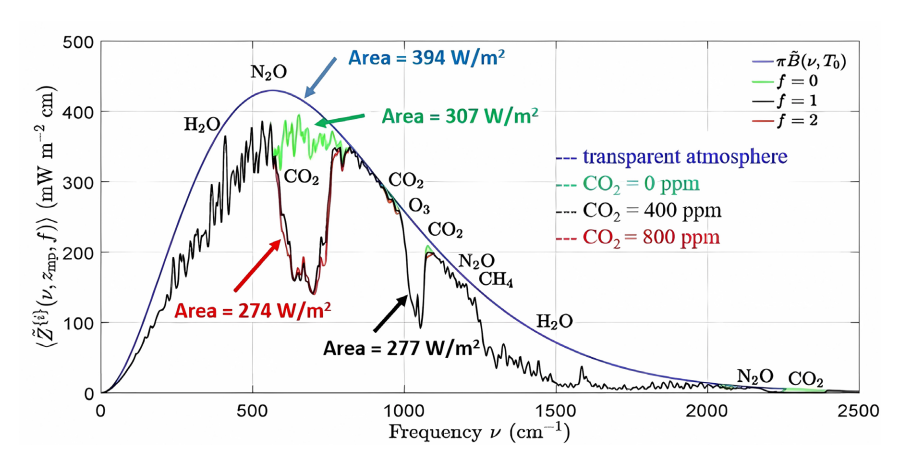


Figure 17. Total atmospheric absorptivity changes by CO₂ increases calculated by Wijngaarden and Happer [2].

Ground measurements fall in line with Figure 17 and indicate almost complete

saturation of IR absorption in our atmosphere. We were therefore interested in designing a simple and independent low-cost experimental setup to demonstrate this saturated behavior. This setup and the results obtained will be described in the following section.

2. Experimental Methods

The aim of this work was therefore to demonstrate in a simple manner that an IR-active gas can indeed influence the heat radiation of a body. Another aim was to demonstrate that CO_2 back-radiation is limited by saturation of absorbance. This was realized by two different experimental setups.

The measurements should allow us to learn if the saturation behavior measured by others and discussed in the foregoing sections of this work are indeed correct and draw conclusions towards the question of CO₂-induced global warming.

According to the second law of thermodynamics, heat flows from hotter to colder objects ("downhill"), unless energy in some form is supplied to reverse the direction of heat flow or there is a medium that absorbs part of the energy and remits it isotropic, like greenhouse models describe the radiation household within our atmosphere. Our test atmospheres were studied against a -25° C cooled black disc ("Lab Mode") or a cloudless night sky ("Outdoor or Field Mode") using the natural IR source of surface and atmospheric back radiation.

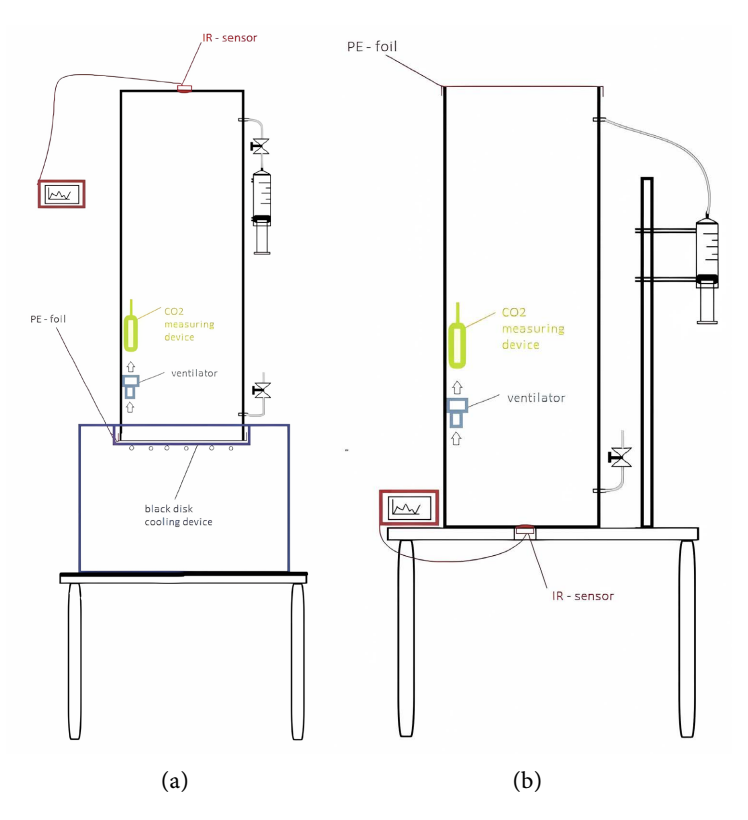


Figure 18. experimental setup for (a) "Lab Mode" using a cooling compressor and (b) "Field Mode".

Translating these setups into energy flow diagrams like in Figure 3 & Figure 4 we first analyze Figure 18(a).

As shown in **Figure 19** the "Lab Mode" IR sensor response is solely determined by the back-radiation from Test Atmosphere 2 with increasing CO₂ concentrations. The cold plate on the other side of the test cylinder allows thermal flow according to the second law of thermodynamics. Inside the volume of the test cylinder, a CO₂ detector and a low-power ventilator are mounted and run by a combined power pack. The communication with the CO₂ detector is performed via Bluetooth. β is the intensity ratio $\beta = A_D \sin^2 \theta$ for an IR detector with numerical aperture θ within the cylindrical test column and the detector area A_D of 1 cm². ε_2 solely depends on the GH gas concentrations in the test tube and the intensity $\frac{\beta}{2} \varepsilon_1 \varepsilon_2 \sigma T_1^4$ is measured by a Thermopile IR detector from Thorlabs®.

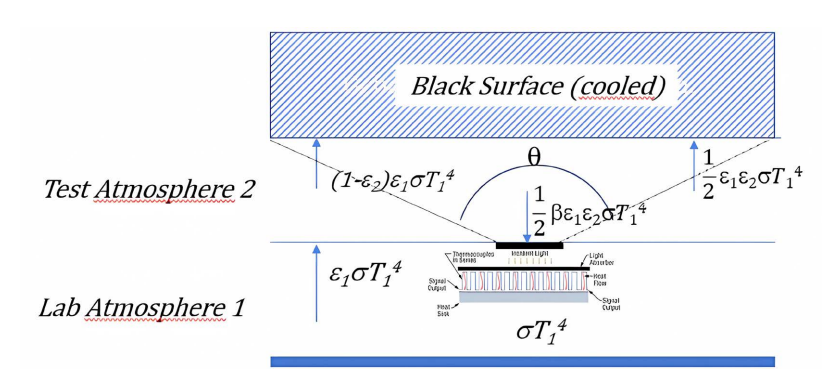


Figure 19. "Lab Mode" test bench with cooled black disc.

In the "Field Mode (**Figure 18(b)**) the test cylinder is rotated by 180°, the cooling compressor is removed and replaced by the clear night sky. The temperature gradient in this case is the difference between T_S and T_E , where T_E is derived from (7)

$$T_E = 4\sqrt{\frac{\left(1 + KC^2\right) \cdot 8.78 \cdot 10^{-13} \cdot T_S^{5.852} \cdot RH^{0.07195}}{\sigma}}$$
(17)

The down-dwelling radiation through the test chamber into the IR detector is determined by

$$P = \beta e_1 e_2 s T_F^4 \tag{18}$$

Using the parametrization of Howard [11] we obtain for CO_2 test atmospheres power densities below the detection limit of the IR sensor of $10 \,\mu\text{W/cm}^2$ in this setup. Using stronger GH gases would significantly increase ε_1 as we have tested in our experimental series. This would prove that CO_2 is a relatively weak greenhouse gas even when increasing its concentration into the percentage region, compared to other GH gases, which would be detectable already at relatively low concentrations.

3. Results

The 7-liter test cylinder in Figure 18(a) was filled up with pure nitrogen. CO₂ was

added in 50 ml steps. Simultaneously the CO₂ detector was used to measure the concentration while the ventilator was trying to homogenize the gas volume admixture. In **Figure 20** the obtained power values of the IR detector are plotted.

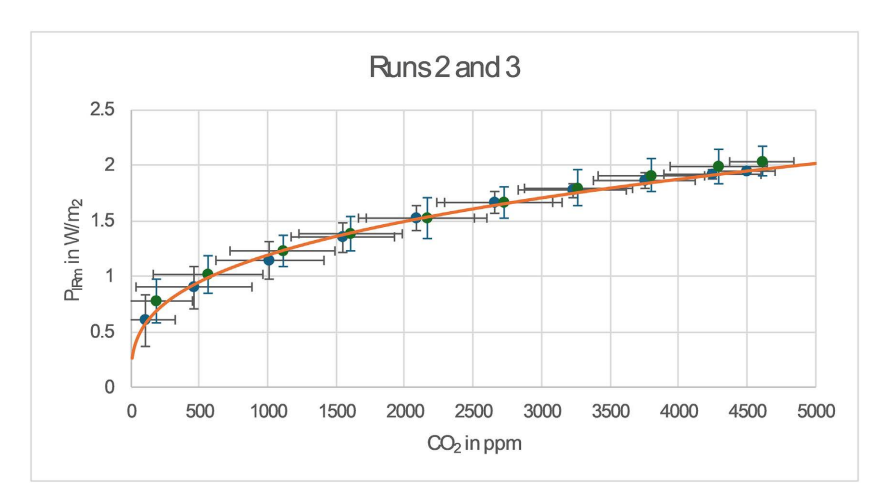


Figure 20. Run 2.2 and Run 2.3 in the Lab Mode mixing CO₂ into a pure nitrogen atmosphere.

From previous considerations, we can estimate the back-radiation by the parametrization of Howard [11] (Equations (14)-(15)).

Low values of absorption length are outside the fit and measurement range of Howard but serve as extrapolations to estimate orders of magnitude. The trend in **Figure 21** is indeed very similar to the measured values in **Figure 20** and confirms the logarithmic behavior of the absorption.

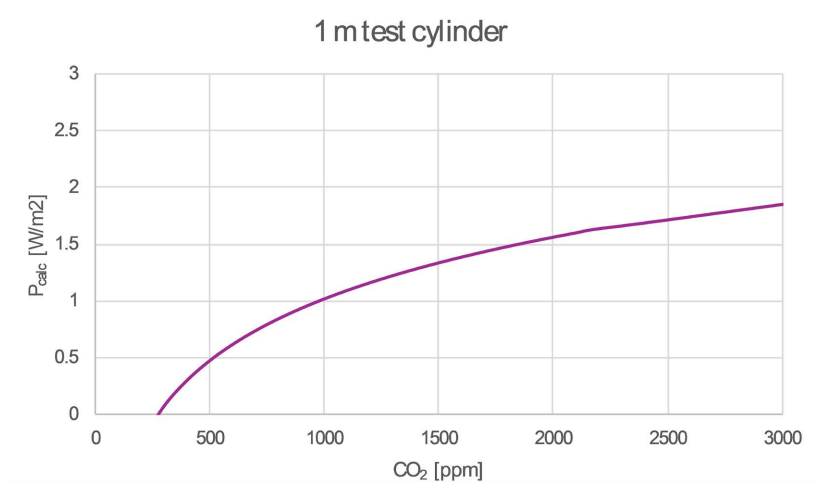


Figure 21. P calculated from Howard [11].

Using the values plotted in Figure 20 we can estimate the fractional absorbance A_f for varying CO₂ concentrations in N₂ atmospheres

$$\ln\left(\frac{I_0}{I_1}\right) = \varepsilon \cdot c \cdot d \tag{19}$$

where c is the molar concentration (mol·m⁻³) and d air column length (m). We use the Beer-Lambert law (13) function, where ε is the absorption coefficient of our test atmosphere to obtain

$$A_f = \frac{I_o - I}{I} = \left(1 - e^{-\varepsilon \cdot c \cdot d}\right) \tag{20}$$

Using (20) it is possible to calculate the back-radiation for a given air column length (Figure 22) at ground-level conditions for saturation at a given ppm CO₂.

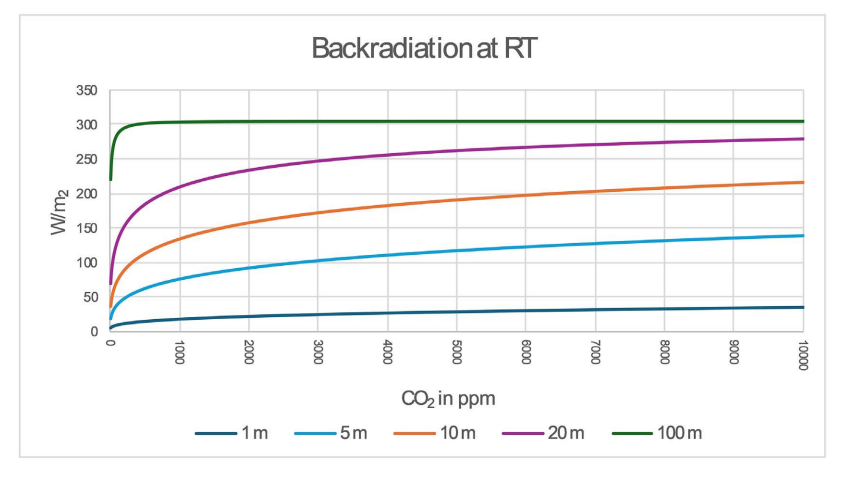


Figure 22. Calculated back-radiation for different long air columns at room temperature (RT).

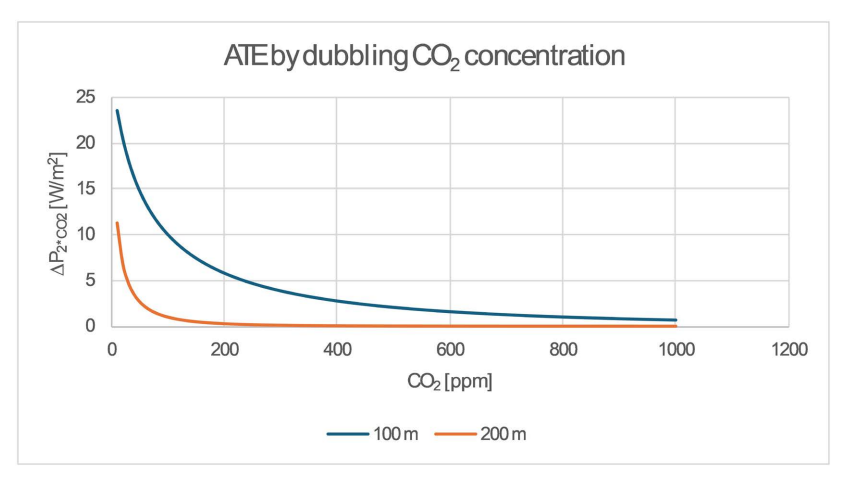


Figure 23. Calculated effect of CO₂ doubling on backscattered power in two air columns.

In Figure 23 we calculated the corresponding atmospheric thermal enhancement (ATE) when doubling the actual CO_2 concentration for a homogeneous atmosphere of 100 m thickness at 1 bar. The result shows a rapid reduction in ATE with increasing the length of the air columns. Applying this result to the real world means saturation in CO_2 concentration with respect to measurable thermal effects. This will be discussed in more detail in the next chapter.

Figure 24 was the result obtained in the so-called Field Measurements against a black cloudless night sky. There is a clear indication that no measurable

backscattering is observable when adding CO₂ from 0 to 5000 ppm to the system. Equation (9) with ε_1 -0.2, ε_2 < 0.2 and β -0.02 gives $\beta \varepsilon_1 \varepsilon_2$ < 0.0004 and therefore $P = \beta \varepsilon_1 \varepsilon_2 \sigma T_E^4 < 3 \times 10^{-2} \text{ W/m}^2 = 3 \text{ µW/cm}^2$. The working power of the used Thermopile Thorlabs detector with 1 cm² active area starts at 10 µW. For stronger GH gases it would be possible to exceed the detection limits and obtain a response. This was shown by using the Freon gas $C_2H_2F_4$ as shown in the next figure.

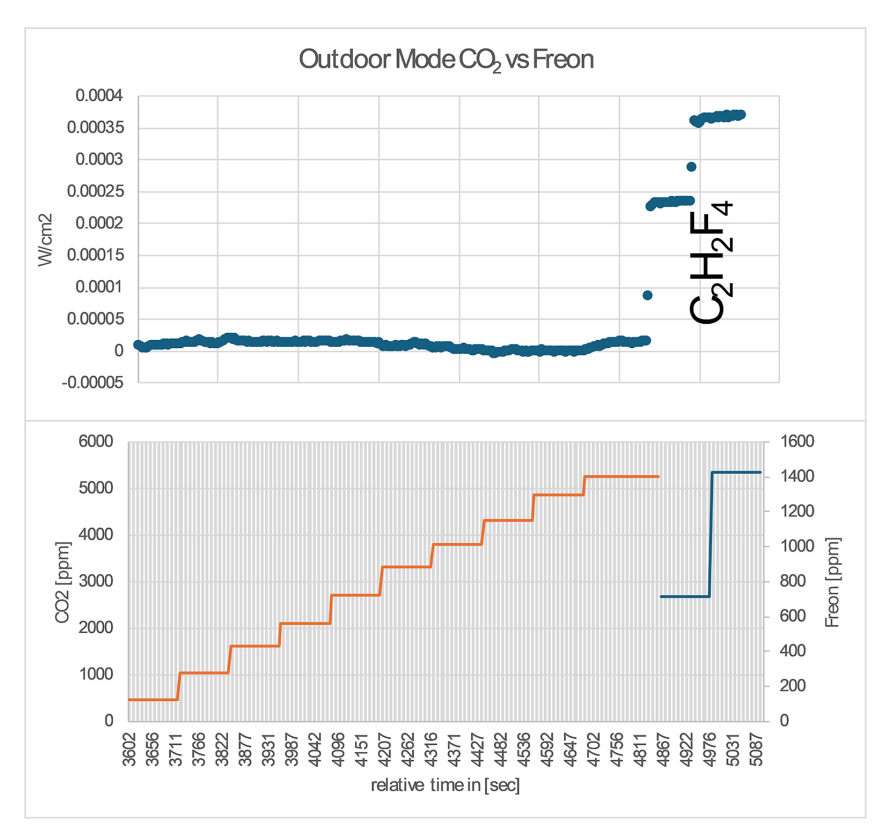


Figure 24. Field Mode comparative measurement CO₂ and Freon (C₂H₂F₄).

The detector was indeed reacting when $C_2H_2F_4$ Freon was added up to 1400 ppm. The measured absorbance of $C_2H_2F_4$ by NIST [15] (**Figure 25**) is indeed, up to 100 times stronger than CO_2 measured by the same institution [16] (**Figure 26**).

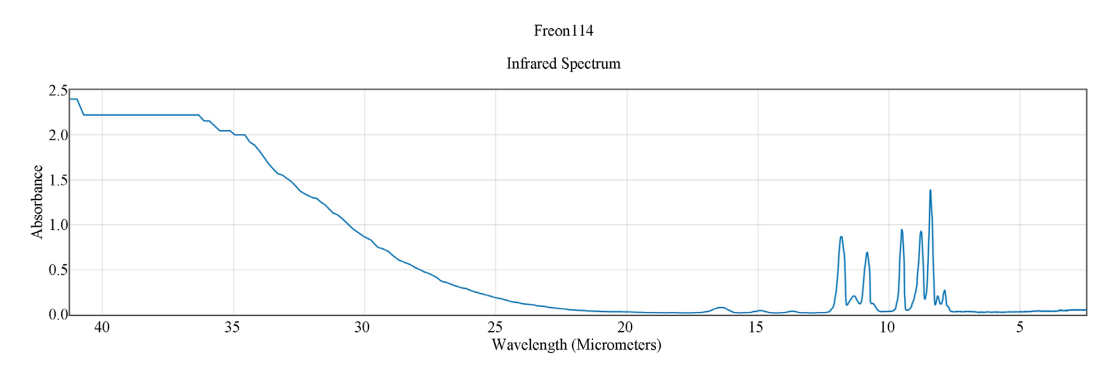


Figure 25. Absorbance of Freon (C₂H₂F₄) [15].

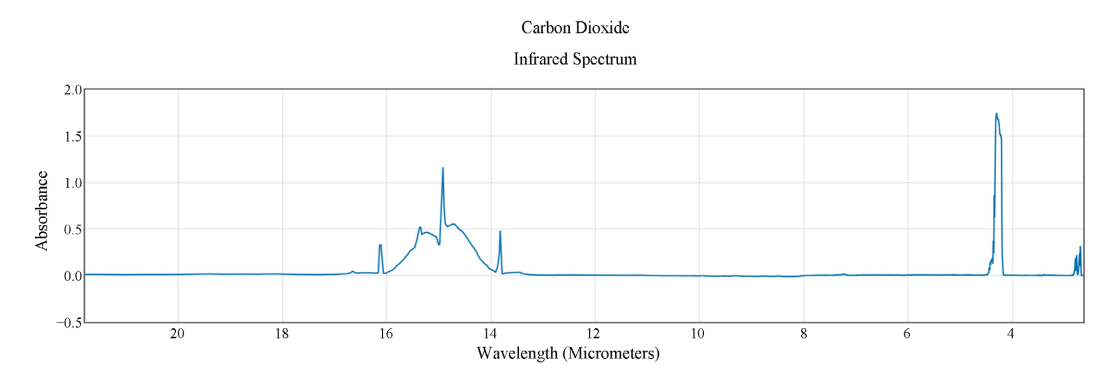


Figure 26. Absorbance of carbon dioxide (CO₂) [16].

4. Discussion

Atmospheric windows, especially the optical and infrared, affect the distribution of energy flows and temperatures within Earth's energy balance. The windows depend upon clouds, water vapor, trace greenhouse gases, and other components of the atmosphere.

Out of an average of 341 watts per square meter (W/m²) of solar irradiance at the top of the atmosphere, about 161 W/m² reaches the surface via atmospheric windows and through clouds (albedo). IR absorption by the atmosphere and corresponding atmospheric heating leads to an equilibrium of 333 W/m² of backradiation and outgoing LW surface radiation of 396 W/m² latent heat from evaporation (80 W/m²) and other thermal losses (17 W/m²). Our measurements align with limitations to an increase of maximum 3W/m² back-radiation by doubling the CO₂ content from 400 to 800 ppm. This minor contribution should not exceed a temperature increase of more than $0.5\,^{\circ}$ K a value, which is not within the range of significant impact for climatic changes and much lower than annual temperature variations in all regions of the earth.

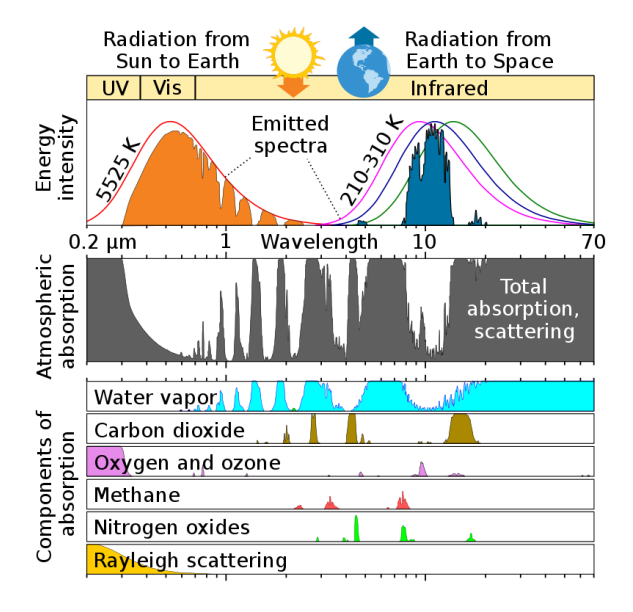


Figure 27. "The Atmospheric Window", NOAA [17] [18].

425

From Figure 27 it should be obvious that only minor contributions can be obtained from the edges of the two prominent CO₂ windows. Water vapor is indeed the major absorber and other GH gases are not relevant at their current concentrations. Increased water vapor should also lead to cloud coverage at constant aerosol concentrations. Slight variations of solar constants and cosmic rays using balanced feedback loops should allow for long-term thermal equilibrium. Fluctuations are often due to unnatural time scales, long-time constants, and statistical noise. In a simplified picture, where we consider an atmosphere with uniform density corresponding to the surface density $\rho = 1.2225 \text{ kg} \cdot \text{m}^{-3}$ we obtain an atmospheric air column weight of 10,300 kg·m⁻² at a length of 8425 m. From our measurements and a simple Beer-Lambert model of such an air column, we found (Figure 13) already at 200 m complete saturation at current CO₂ concentrations, without significant contributions to further ATE. Schildknecht [19] using similar arguments finds that doubling of the CO₂ content in air from 380 ppm to 760 ppm in one century is an increase of $\Delta T \simeq 0.5$ °C, which corresponds well with the expected values of this and other works.

Our results should therefore contribute to previously accepted findings which do not indicate any reason to cause climate run-aways by increased CO₂ contents. Ekholm [20] introduced the idea of fictitious atmospheric radiation levels due to CO₂ increase. According to him secular cooling of the earth is the principal cause of variation in the quantity of carbon dioxide in the atmosphere. He explained how carbon dioxide is a key player in the greenhouse effect and how his conclusion was based on the earlier work of Fourier, Pouillet, Tyndall, and others. According to their estimations, a tripling of carbon dioxide levels will raise global temperatures by 7°C to 9°C. An increase in carbon dioxide should heat high latitudes more than the tropics and create a warmer more uniform climate over the entire Earth. Hansen [21] testified this before Congress and raised public awareness of climate change. Hansen was claiming "The most powerful feedback is provided by water vapor". While this argument seems strong it must be questioned considering paleoclimatic facts e.g. higher temperatures in the Eemian interglacial period 120,000 years ago and the Holstein interglacial period 5,000 to 15,000 years ago did not trigger a tipping point or a galloping greenhouse effect. Sarker [22] mentions correctly that 0.24 gigatons of carbon were emitted into the atmosphere for 50,000 years to cause this severe warming known as the PETM. In comparison, humans emit 10 gigatons, or approximately fifty times that amount of carbon annually, into the atmosphere. There is no doubt that a warming climate has negative impacts on various important properties, such as the aridity index for rivers [23]. Even just studying rivers there are many other anthropogenic impacts not related to CO2 which dramatically influence their current and future environmental integrity [24] [25]. Current global warming can be natural and/or anthropogenic. To be sure, we must understand how it was possible to obtain 100 m higher sea levels or to end up by glaciation over large areas of landmasses without anthropogenic CO₂ emission triggers. Additional energy or energy loss was due to natural forces which must be fully understood before drawing wrong conclusions. Ice core data do not indicate fundamental different temperature variations over the last 10,000 years. We also need a better understanding of the validity of power flow diagrams as published by the IPCC. It would be a great success of our efforts if such questions could be reconsidered also considering the results presented in this work.

5. Conclusion

Experimental evidence in this work confirms earlier work that increasing levels of CO₂ at current levels in the atmosphere cannot significantly contribute to warming by more back-radiation. We also demonstrated that increasing greenhouse spurious gases like Freon show a strong response in back-radiation when added into our atmospheric test chamber. Climate models and their CO₂ forcings should be revised and much more experimental evidence about the IR radiation response of greenhouse gases should be collected before appointing current warming trends and climate change mechanisms monocausal to greenhouse gas theories.

Conflicts of Interest

The authors declare no conflicts of interest regarding the publication of this paper.

References

- [1] European Parliament (2023) Fortschritte der EU bei der Verwirklichung ihrer Klimaziele für 2020 (Infografik).

 https://www.europarl.europa.eu/news/de/headlines/society/20180706STO07407/for tschritte-der-eu-bei-der-verwirklichung-ihrer-klimaziele-infografik?at campaign=2
 0234-Green&at medium=Google Ads&at platform=Search&at creation=DSA&at goal=TR G&at audience=&at t
- [2] van Wijngaarden, W.A. and Happer, W. (2020) Dependence of Earth's Thermal Radiation on Five Most Abundant Greenhouse Gases. arXiv: 2006.03098. https://doi.org/10.48550/arXiv.2006.03098
- [3] Happer, W. and Lindzen, R. (2022) Comment and Declaration on the SEC's Proposed Rule "The Enhancement and Standardization of Climate-Related Disclosures for Investors," File No. S7-10-22, 87 Fed. Reg. 21334. https://www.sec.gov/comments/s7-10-22/s71022-20132171-302668.pdf
- [4] Barrett, J. (2005) Greenhouse Molecules, Their Spectra and Function in the Atmosphere. *Energy & Environment*, 16, 1037-1045. https://doi.org/10.1260/095830505775221542
- [5] James, I.N. (1994). Introduction to Circulating Atmospheres. Cambridge University Press. https://doi.org/10.1017/cbo9780511622977
- [6] https://web.archive.org/web/20230329191117/www.acs.org/climatescience/atmosphericwarming/multilayermodel.html
- [7] Swinbank, W.C. (1963) Long-Wave Radiation from Clear Skies. *Quarterly Journal of the Royal Meteorological Society*, 89, 339-348.
 https://doi.org/10.1002/qj.49708938105
- [8] Goforth, M.A., Gilchrist, G.W. and Sirianni, J.D. (2002) Cloud Effects on Thermal Downwelling Sky Radiance. *Proceedings of SPIE-The International Society for*

- *Optical Engineering* 4710, Orlando, 15 March 2002. https://doi.org/10.1117/12.459570
- [9] Petty, G.W. (2006) A First Course in Atmospheric Radiation. Sundog Publishing, 223.
- [10] Angström, A. (1918) Smithsonian Inst., Misc. Coll., 65, 3. https://www.realclimate.org/images/Angstrom.pdf
- [11] Howard, J.N., Burch, D.E. and Williams, D. (1956) Infrared Transmission of Synthetic Atmospheres II Absorption by Carbon Dioxide. *Journal of the Optical Society of America*, **46**, 237-241. https://doi.org/10.1364/josa.46.000237
- [12] Fröhlich, C., Philipona, R. and Marty, C. (1998,) Untersuchung des Oberflächenstrahlungshaushaltes in den Alpen und im Vergleich zum schweizerischen Mittelland. VDF Hochschulverlag AG an der ETH Zürich.
- [13] Makhdoumi Akram, M., Nikfarjam, A., Hajghassem, H., Ramezannezhad, M. and Iraj, M. (2020) Low Cost and Miniaturized NDIR System for CO₂ Detection Applications. *Sensor Review*, **40**, 637-646. https://doi.org/10.1108/sr-06-2019-0140
- [14] Harde, H. (2014) Advanced Two-Layer Climatemodel for the Assessment of Global Warming by CO₂. *Open Journal of Atmospheric and Climate Change*, **1**, 1-51.
- [15] C₂Cl₂F₄.

 https://webbook.nist.gov/cgi/cbook.cgi?ID=C76142&Type=IR-SPEC&Index=2
- [16] CO₂.

 https://webbook.nist.gov/cgi/cbook.cgi?ID=C124389&Units=SI&Type=IR-SPEC&Index=1#IR-SPEC
- [17] National Oceanic and Atmospheric Administration (2023) The Atmospheric Window. https://www.noaa.gov/jetstream/satellites/absorb
- [18] US Department of Commerce, NOAA. The Earth-Atmosphere Energy Balance. https://www.weather.gov/
- [19] Schildknecht, D. (2020) Saturation of the Infrared Absorption by Carbon Dioxide in the Atmosphere. *International Journal of Modern Physics B*, **34**, Article 2050293. https://doi.org/10.1142/s0217979220502938
- [20] Ekholm, N. (1901) On the Variations of the Climate of the Geological and Historical Past and Their Causes. *Quarterly Journal of the Royal Meteorological Society*, **27**, 1-62. https://doi.org/10.1002/qj.49702711702
- [21] Hansen, J., Johnson, D., Lacis, A., Lebedeff, S., Lee, P., Rind, D., et al. (1981) Climate Impact of Increasing Atmospheric Carbon Dioxide. Science, 213, 957-966. https://doi.org/10.1126/science.213.4511.957
- [22] Sarker, S. (2022) Fundamentals of Climatology for Engineers: Lecture Note. *Eng*, **3**, 573-595. https://doi.org/10.3390/eng3040040
- [23] Sarker, S. (2021) Investigating Topologic and Geometric Properties of Synthetic and Natural River Networks under Changing Climate. https://stars.library.ucf.edu/etd2020/965
- [24] Gao, Y., Sarker, S., Sarker, T. and Leta, O.T. (2022) Analyzing the Critical Locations in Response of Constructed and Planned Dams on the Mekong River Basin for Environmental Integrity. *Environmental Research Communications*, **4**, Article 101001. https://doi.org/10.1088/2515-7620/ac9459
- [25] Sarker, S., Veremyev, A., Boginski, V. and Singh, A. (2019) Critical Nodes in River Networks. Scientific Reports, 9, Article No. 11178. https://doi.org/10.1038/s41598-019-47292-4